Asian Journal of Chemistry; Vol. 29, No. 11 (2017), 2391-2395

ASIAN JOURNAL OF CHEMISTRY

https://doi.org/10.14233/ajchem.2017.20690

Structural and Optical Characterization of ZnO-TiO_2-SiO_2 Nanocomposites Synthesized by Sol-Gel Technique

DHARM VEER[1], RAM MEHAR SINGH[1] and HARISH KUMAR[2,*]

[1]Material Science Laboratory, Department of Physics, Ch. Devi Lal University, Sirsa-125 055, India
[2]Material Science & Electrochemistry Laboratory, Department of Chemistry, Ch. Devi Lal University, Sirsa-125 055, India

*Corresponding author: E-mail: harimoudgil1@gmail.com

Received: 5 April 2017; *Accepted*: 29 June 2017; *Published online*: 29 September 2017; AJC-18557

ZnO-TiO_2-SiO_2 nanocomposites were synthesized by sol-gel technique. Nanocomposites were annealed at 400 °C. The structural and optical characterization was performed by XRD, TEM, FTIR and UV-visible spectroscopic techniques. Average particle size of ZnO-TiO_2-SiO_2 nanocomposites was found to be 34.23 nm using XRD technique. The energy band gap of ZnO, TiO_2 and ZnO-TiO_2-SiO_2 were found to be 3.4, 3.6 and 3.5 eV, respectively.

Keywords: Zinc oxide, Nickel oxide, Nanocomposites, Sol-gel technique, Metal nanoparticles.

INTRODUCTION

Metal oxide nanoparticles attract great attention in recent year on account of their special electronic and chemical properties. Among the metal oxide semiconductor, TiO_2 and ZnO were investigated extensively due to their chemical stability and efficient photocatalytic properties. Zinc oxide is II-VI semiconductor with Wurtzite structure [1] having large band gap (3.37 eV at room temp.) and high exiton binding energy (60 meV) that is optically transparent for visible light [2], has been intensively studied for its versatile physical properties and promising potential applications [3]. Zinc oxide is widely used in different areas because of its unique photo catalytic, electrical, electronic, optical, electrical conductivity, UV-blocking, photo oxidizing, dermatological, antibacterial properties [4-10] and self sterilization [11-16]. Moreover, ZnO nanoparticles are safe material for human and have been applied in personal care products [17,18]. Titanium dioxide (TiO_2) nanoparticles, a functional semiconductor with an electronic band gap of 3.3 eV is one of the most extensively studied materials due to its catalytic, electrical, optoelectronic and cosmetology applications.

The composites of ZnO and TiO_2 have useful applications in photocatalysis. TiO_2 is functional semiconductor with an electronic band gap of 3.3 eV and is one of the most extensively studied materials due to its catalytic, electrical, optoelectronics properties. ZnO nanoparticles are also used as semiconductor and also as a piezoelectric material with a direct band gap of 3.4 eV.

In this paper, we have synthesized ZnO-TiO_2-SiO_2 nanocomposites. Structural and optical characterizations were carried out by X-ray diffraction (XRD), TEM, FTIR and UV-visible spectroscopy techniques.

EXPERIMENTAL

Equimolar solution of $ZnCl_2$ and TiO_2 were taken in borosil beaker of 500 mL capacity. The reaction mixture was acidified by adding concentrated HNO_3 drop by drop to make pH between 1-2. A gel of TEOS and ethanol was prepared by mixing in 1:4 molar ratio. Acidified solution of $ZnCl_2$ and TiO_2 was added drop wise to alcoholic gel with gentle stirring over a period of 6 h maintained at a constant temperature of 70 °C. Now prepared sol is filled in Petri plates and put in oven for 10 days at 100 °C after that they are kept in muffle furnace maintained at a constant temperature of 400 °C for 4 h.

Characterization techniques: Structural and optical properties of ZnO-TiO_2-SiO_2 nanocomposites were carried out by X-ray diffraction (XRD) (Panalytical's X'pert Pro using Cu-$K_{\alpha 1}$, λ = 0.151406 nm radiations), transmission electron microscopy (TEM) (Tecnai 200KV Fei Electron Optics λ = 35 nm), infrared spectroscopy (FTIR) (Shimadzu, IR Affinity-1) in the wavelength range of 4000-400 cm^{-1} and UV-visible spectroscopy (Nanodrop-2003, Thermo-scientific company) in the wavelength range of 200-800 nm.

RESULTS AND DISCUSSION

Structural and optical characterization of ZnO and TiO_2 nanoparticles and ZnO-TiO_2-SiO_2 nanocomposites

ZnO nanoparticles: Fig. 1 shows the X-ray diffraction pattern of ZnO nanoparticles. The all detectable peaks could be clearly identified as characteristic peaks are at an angle of 31.4, 34.5, 36.3, 47.6, 56.7, 62.9, 66.4, 68.0, 69.2, 72.6 and 77.0° indexed as (100), (002), (101), (102), (110), (103), (200), (112), (201), (004) and (202) crystal planes respectively. All these diffraction peaks corresponds to the hexagonal Wurtzite structure of zinc oxide nanoparticles (lattice parameter a = 3.27 Å and c = 5.0 Å) in accordance with the standard spectrum (JCPDS, Card file No.05-0664).

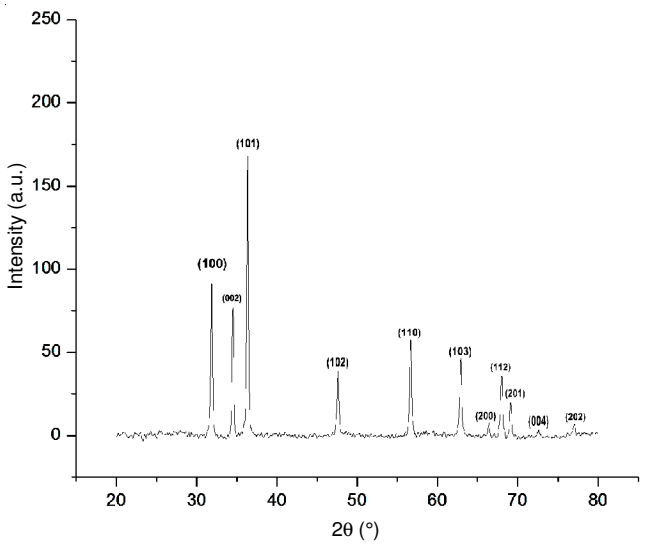

Fig. 1. X-ray diffraction pattern of ZnO nanoparticle

Grain size of ZnO nanoparticles was calculated by Debye Scherrer's formula given in eqn. (1).

$$d = k\lambda/\beta \cos\theta \quad (1)$$

where, k is polarization (shape) factor, λ wavelength of light (λ = 1.542 Å) (CuK_α), β is the full width at half maximum (FWHM) of the line and θ is the diffraction angle. The particle size corresponding to highest intensity peak was found to be 44.88 nm.

TiO_2 nanoparticles: Fig. 2 shows the XRD diffraction pattern of TiO_2 nanoparticles. The characteristic peaks were observed at 2θ angles of 25.3, 37.8, 48.1, 53.9, 55.1, 62.7, 68.8, 70.3 and 75.1° corresponding to (101), (004), (200), (105), (211), (204), (116), (220), (215) crystal planes, which confirms the formation of anatase phase of Titania which is in accordance with the standard diffraction pattern (JCPDS-78-1510). The particle size corresponding to highest intensity peak was found to be 43.71 nm.

ZnO-TiO_2-SiO_2 Nanocomposites: Fig. 3 shows the X-ray diffraction pattern of ZnO-TiO_2-SiO_2 nanocomposites. The characteristic diffraction peaks were observed at an angle (2θ) of 25.2, 37.7, 47.9, 53.8, 54.9, 62.6, 68.7, 70.2, 75.0° corresponds to the crystal planes of (101), (004), (200), (105), (211), (204), (116), (220), and (215) indicating the formation

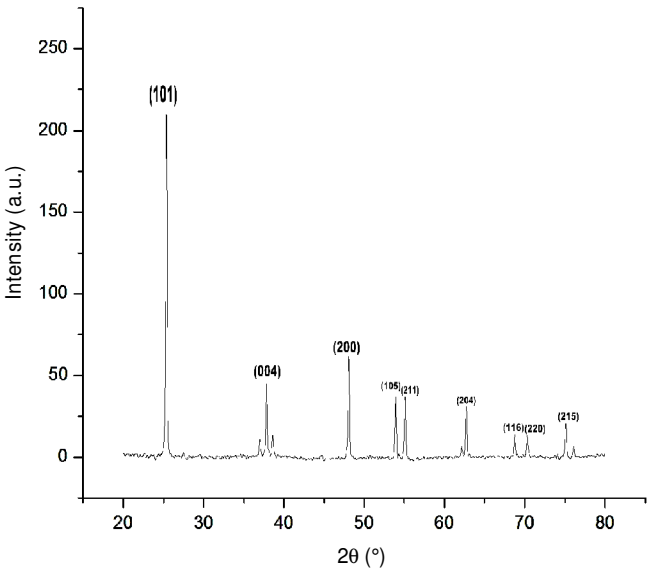

Fig. 2. X-ray diffraction pattern of TiO_2 nanoparticle

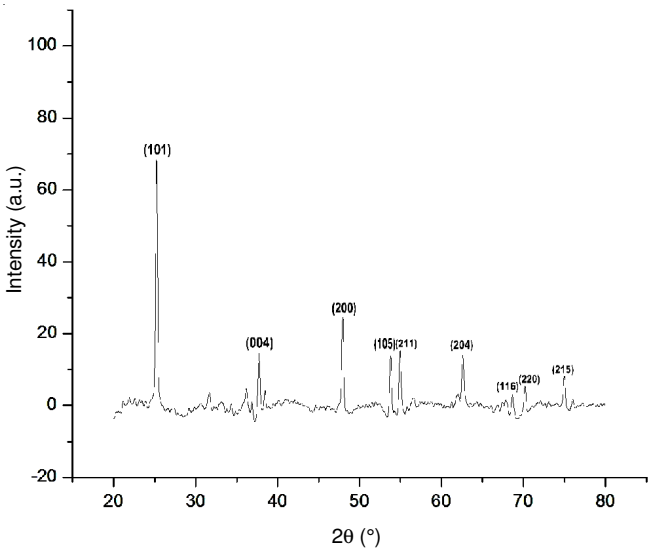

Fig. 3. X-ray diffraction pattern of ZnO-TiO_2-SiO_2 nanocomposites

of anatase structure of TiO_2 in naocomposite (JCPDS card No. 78-1510). In addition, peaks at 2θ angle of 31.6, 34.8, 36.7, 48.4, 63.0, 69.1 and 75.4° corresponds to the crystal planes of (100), (002), (101), (102), (103), (201) and (202) indicates the information of Wurtzite structure of ZnO in nanocomposite (JCPDS card No. 36-1451). The average particle size corresponding to dominating peak in diffraction pattern was found to be 43.71 nm.

Strain calculation using W-H plot: The strain induced in powders due to crystal imperfection and distortion was calculated using the formula given in eqn. 2.

$$\varepsilon = \beta/4 \tan\theta \quad (2)$$

From eqns. 1 and 2, it was confirmed that the peak width from crystallite size varies as 1/cos θ and strain in the crystal varies as tan θ.

Fig. 4 shows W-H plot of ZnO and TiO_2 nanoparticles, respectively. Fig. 5 shows W-H plot of ZnO-TiO_2-SiO_2 nanocomposite.

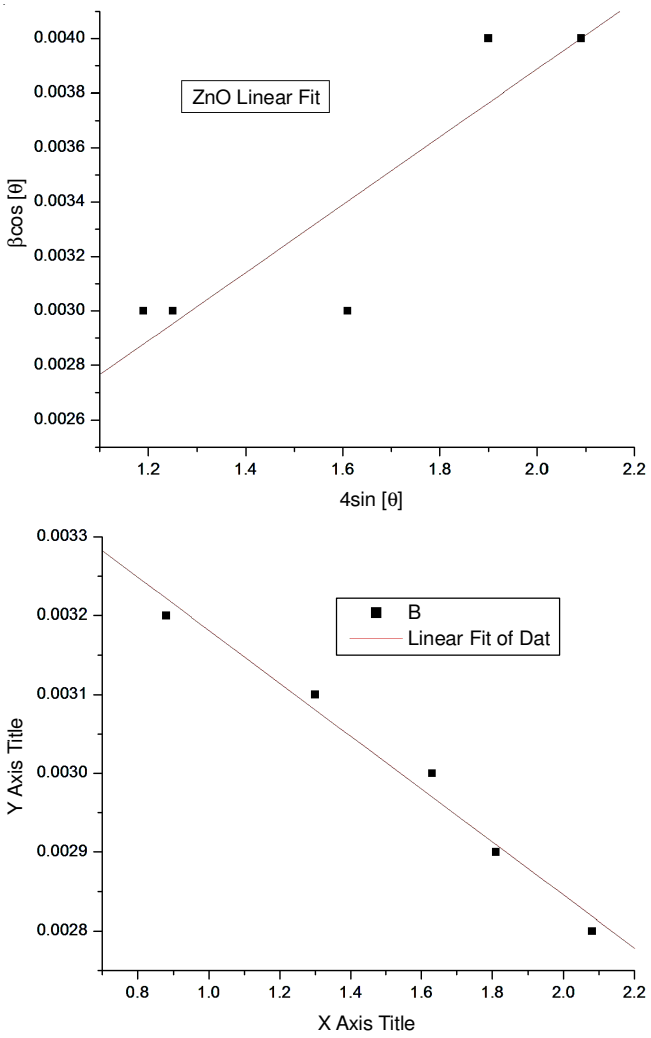

Fig. 4. W-H plot of ZnO and TiO_2 nanoparticles respectively

Assuming that the crystallite size and strain contributions to line broadening are independent to each other and both have a Cauchy-like profile, the observed line breadth is simply the sum of eqns. 1 and 2.

$$\beta = K\lambda/d\cos\theta + 4\varepsilon\tan\theta \quad (3)$$

By rearranging the above equations, we get

$$\beta\cos\theta = K\lambda/d + 4\varepsilon\tan\theta \quad (4)$$

The above equations are popularly known as W-H equations.

From W-H equations, particle size can be found as d = Kλ/intercept.

The negative slope of the fitted line in a Williamson-Hall plot (Figs. 4b and 5) indicates the presence of a compressive strain in the crystal lattice of the specimen, while a positive slope (Fig. 4a) indicates a tensile strain.

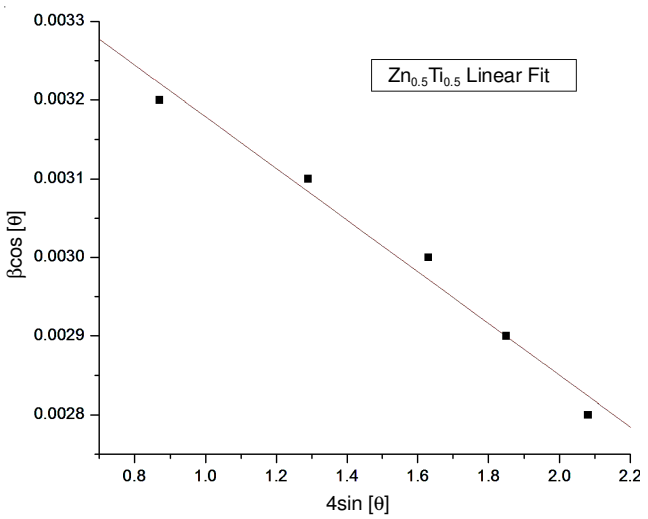

Fig. 5. W-H plot of ZnO-TiO_2-SiO_2 nanocomposite

TEM analysis of pure and ZnO-TiO_2-SiO_2 nanocomposites: Figs. 6-8 show the TEM images of zinc oxide, titanium dioxide nanoparticles and ZnO-TiO-SiO_2 nanocomposites, respectively. The microstructural characterization studies were conducted to determine the size of nanoparticles and nanocomposites and also to examine the homogeneity and size distribution. The particles were observed to be almost spherical. The mean particle size of ZnO, TiO nanoparticles and ZnO-TiO-SiO_2 nanocomposites were found to be 40, 80 and 120 nm, respectively.

Fourier transform infrared spectroscopy (FTIR): Fig. 9 shows the infrared absorption spectra of ZnO nanoparticles in the range of 4000-400 cm^{-1}. The band at 3485 cm^{-1} indicates the presence of asymmetric stretching –OH bond. The band near 2372 cm^{-1} indicates the presence of bending vibration of

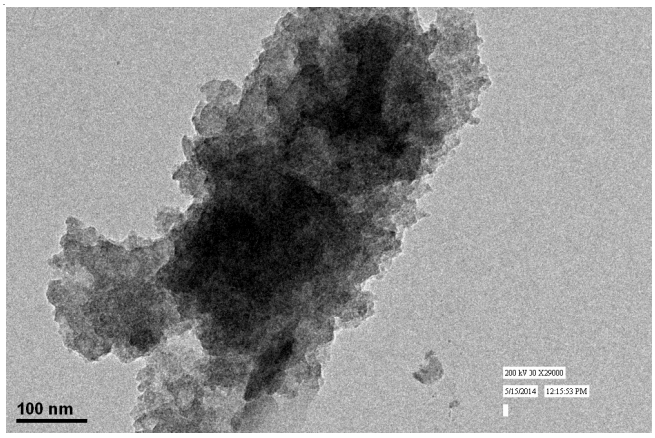

Fig. 6. TEM image of ZnO nanoparticles

TABLE-1
AVERAGE PARTICLE SIZE, LATTICE STRAIN, LATTICE PARAMETERS, INTER PLANAR SPACING AND DISLOCATION DENSITY OF ZnO, TiO_2 AND ZnO-TiO_2-SiO_2 NANOCOMPOSITES

Sample	Particle size (nm)			Lattice strain (ε, a.u.)	Lattice parameters (Å)	Inter planar spacing (d, Å)	Dislocation density
	Debye Scherrer's formula	Williamson-Hall plot method	TEM				
ZnO	44.88	49.55	80-150	1.25×10^{-4}	a = 3.24, c = 5.2	2.60	4.07×10^{-4} $(nm)^{-2}$
TiO_2	43.71	42.43	40-60	4.0×10^{-4}	a = 3.75, c = 9.3	3.51	5.55×10^{-4} $(nm)^{-2}$
Zn-TiO_2-SiO_2	43.70	42.30	80-150	4.0×10^{-4}	a = 3.75, c = 9.3	3.53	5.58×10^{-4} $(nm)^{-2}$

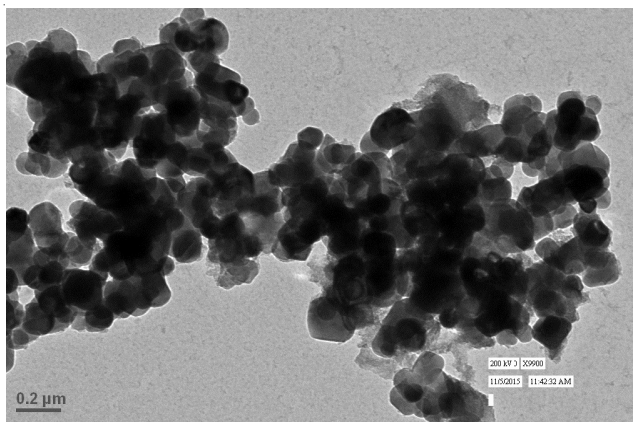

Fig. 7. TEM image of TiO_2 nanoparticles

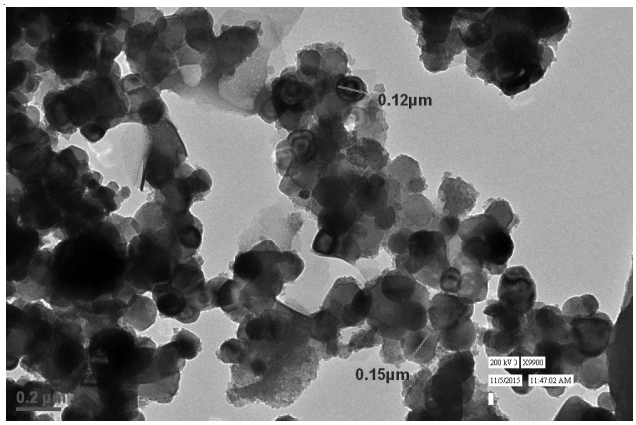

Fig. 8. TEM image of ZnO-TiO_2-SiO_2 nanocomposite

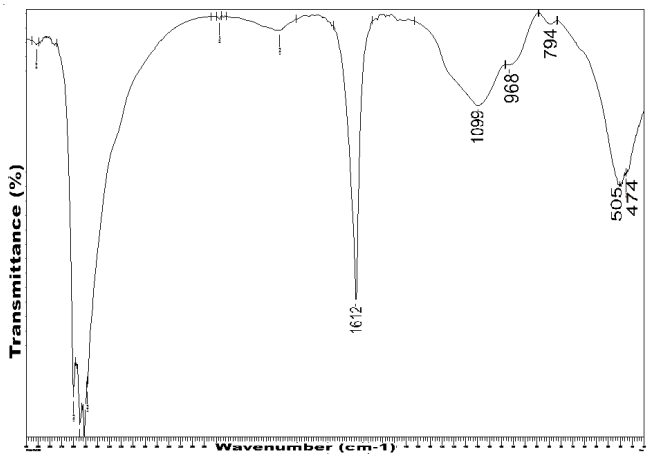

Fig. 9. FTIR spectra of ZnO nanoparticles

O=C=O bond. The band at 1612.49 cm^{-1} is due to the symmetric C = O stretching of zinc chloride. The weak bands at 1099.43, 968.27 and 794.67 cm^{-1} are due to C-O stretching vibration. The absorption bands at 474.49 and 505.35 cm^{-1} corresponds to Zn-O stretching.

Fig. 10 shows the infrared absorption spectra of TiO_2 nanoparticles in the range of 4000-400 cm^{-1}. The FTIR peaks of TiO_2 are at 457, 661, 1083, 2034, 2285, 2860, 2927 and 3425 cm^{-1}. Peaks at 457, 661 and 1083 cm^{-1} corresponds to Ti-O vibrations, peaks at 2034, 2285, 2860 and 2927 cm^{-1} due to C-H stretching vibrations. Peak at 3425 cm^{-1} due to O-H stretching and bending vibrations.

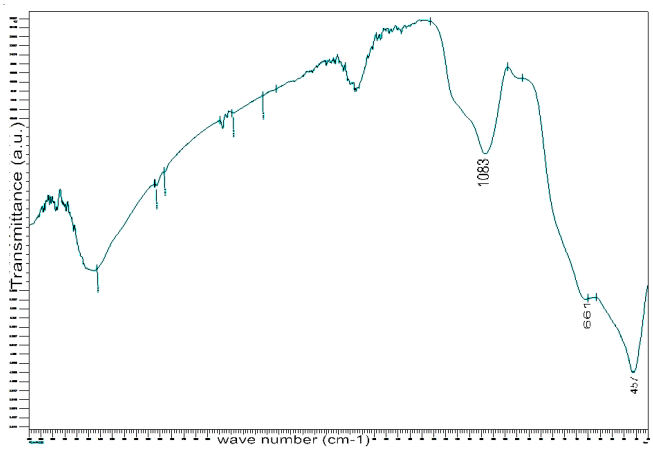

Fig. 10. FTIR spectra of TiO_2 nanoparticles

Fig. 11 shows the infrared absorption spectra of ZnO-TiO_2-SiO_2 particles in the range of 4000-400 cm^{-1}. The absorption peak at 3564, 3480, 3414 and 3200 cm^{-1} for stretching vibration of –OH group. The peaks at 422.4, 443.6, 490, 532.3, 597.3 cm^{-1} are for Zn-OH or Ti-OH. The peak 1600 cm^{-1} for H-O-H bending vibrations. Absorption peak at 1086 cm^{-1} shows the Si-O-Si and Si-O-Zn stretching vibrations.

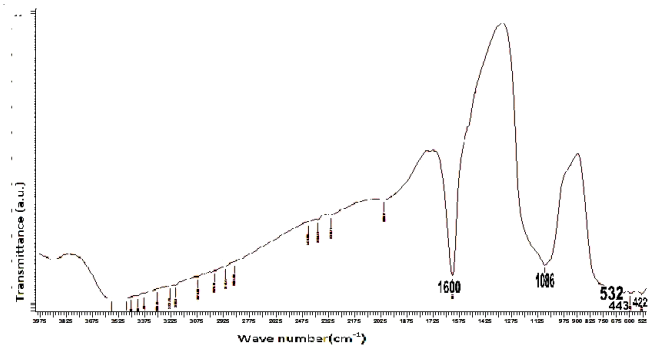

Fig. 11. FTIR spectra of ZnO-TiO_2-SiO_2 nanocomposite

UV-visible absorption spectra of pure ZnO: Fig. 12 shows UV-visible spectrum of ZnO nanoparticles annealed at 400 °C for 4 h. Strong absorption peaks were observed at the wavelength of 240, 280 and 330 nm. Absorption spectrum was investigated to determine the optical properties of nanoparticles.

Energy band gap = $E_g = h\nu = hc/\lambda$

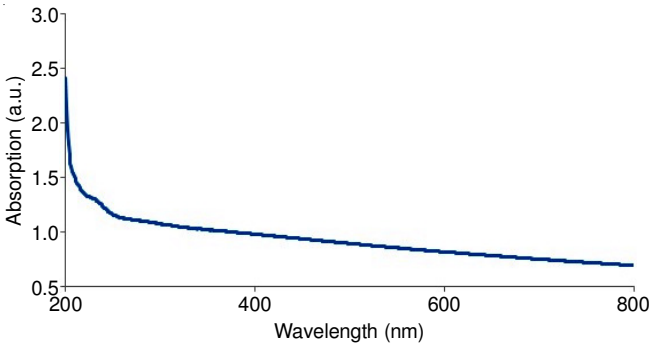

Fig. 12. UV-visible absorption spectrum of ZnO nanoparticle

Optical band gap for TiO_2 nanoparticles was evaluated using the eqn. 5 given as.

$$(\alpha h\nu)^n = A(h\nu - E_g) \quad (5)$$

where α is absorption coefficient, $h\nu$ the photon energy, A is a constant relative to the material and n is either 2 for direct band gap material or ½ for an indirect band gap material.

Figs. 13 and 14 show the UV-visible absorption spectra of TiO_2 nanoparticles and ZnO-TiO_2-SiO_2 nanoparticles, respectively.

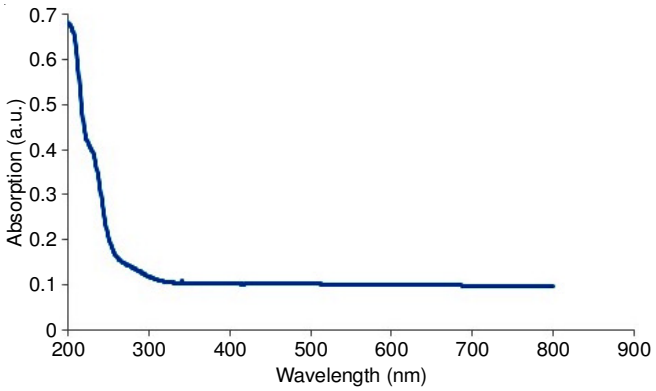

Fig. 13. UV-visible absorption spectrum of TiO_2 nanoparticle

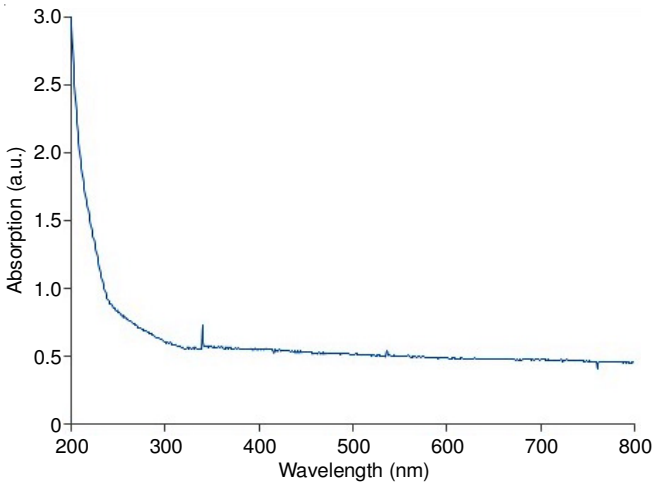

Fig. 14. UV-visible absorption spectrum of ZnO-TiO_2-SiO_2 nanoparticle

According to the equation, the optical band gap for the absorption peak can be obtained by extrapolating the linear portion of the $(\alpha h\nu)^n$ *vs*. $h\nu$ curve to zero. The energy band gap of absorption spectra of ZnO in UV is calculated is 3.4 eV. The energy band gap of absorption spectra of TiO_2 in UV is 3.6 eV. The energy band gap of absorption spectra of ZnO-TiO_2-SiO_2 in UV is 3.5 eV.

Conclusion

ZnO-TiO_2-SiO_2 nanocomposites were synthesized by sol-gel technique. Structural and optical characterization of metal nanoparticles and nanocomposites were carried out using XRD, TEM, FTIR and UV-Visible spectroscopic techniques. Average particle size of ZnO-TiO_2-SiO_2 was found to be 34.23 nm using XRD technique. The energy band gap of ZnO, TiO_2 and ZnO-TiO_2-SiO_2 were found to be 3.4, 3.6 and 3.5 eV, respectively. The absorption bands at 474.49 and 505.35 cm^{-1} corresponds to Zn-O stretching. Peaks at 457, 661 and 1083 cm^{-1} corresponds to Ti-O stretching vibrations. The characteristics peaks at 422.4, 443.6, 490, 532.3, 597.3 cm^{-1} in the finger print region corresponds to Zn-OH and Ti-OH stretching vibrations in Zn-Ti nano-composites. Average particle size, Lattice parameters, inter planar spacing and dislocation density of ZnO, TiO_2 and ZnO-TiO_2-SiO_2 nanocomposites were also calculated from X-ray diffraction study.

REFERENCES

1. J. Lu, Z. Ye, L. Wang, J. Huang and B. Zhao, *Mater. Sci. Semicond. Process.*, **5**, 491 (2002); https://doi.org/10.1016/S1369-8001(02)00114-2.
2. W. Shen, Y. Zhao and C. Zhang, *Thin Solid Films*, **483**, 382 (2005); https://doi.org/10.1016/j.tsf.2005.01.015.
3. D. Djouadi, A. Chelouche, A. Aksas and M. Sebais, *Phys. Procedia*, **2**, 701 (2009); https://doi.org/10.1016/j.phpro.2009.11.013.
4. Z.W. Pan, Z.R. Dai and Z.L. Wang, *Science*, **291**, 1947 (2001); https://doi.org/10.1126/science.1058120.
5. M.S. Arnold, P. Avouris, Z.W. Pan and Z.L. Wang, *J. Phys. Chem. B*, **107**, 659 (2003); https://doi.org/10.1021/jp0271054.
6. J. Sawai, *J. Microbiol. Methods*, **54**, 177 (2003); https://doi.org/10.1016/S0167-7012(03)00037-X.
7. M. Xiong, G. Gu, B. You and L. Wu, *J. Appl. Polym. Sci.*, **90**, 1923 (2003); https://doi.org/10.1002/app.12869.
8. M.A. Behnajady, N. Modirshahla and R. Hamzavi, *J. Hazard. Mater.*, **133**, 226 (2006); https://doi.org/10.1016/j.jhazmat.2005.10.022.
9. E. Tang, G. Cheng, X. Ma, X. Pang and Q. Zhao, *Appl. Surf. Sci.*, **252**, 5227 (2006); https://doi.org/10.1016/j.apsusc.2005.08.004.
10. E. Tang, G. Cheng, X. Ma and X. Pang, *Powder Technol.*, **161**, 209 (2006); https://doi.org/10.1016/j.powtec.2005.10.007.
11. G. Broasca, G. Borcia, N. Dumitrascu and N. Vrinceanu, *Appl. Surf. Sci.*, **279**, 272 (2013); https://doi.org/10.1016/j.apsusc.2013.04.084.
12. M. Montazer and M. Maali Amiri, *J. Phys. Chem. B*, **118**, 1453 (2014); https://doi.org/10.1021/jp408532r.
13. Priyanka and V.C. Srivastava, *Ind. Eng. Chem. Res.*, **52**, 17790 (2013); https://doi.org/10.1021/ie401973r.
14. M. Sudha, S. Senthilkumar, R. Hariharan, A. Suganthi and M. Rajarajan, *J. Sol-Gel Sci. Technol.*, **65**, 301 (2013); https://doi.org/10.1007/s10971-012-2936-y.
15. A. Nazari, M. Montazer, F. Afzali and A. Sheibani, *Clean Technol. Environ. Policy*, **16**, 1081 (2014); https://doi.org/10.1007/s10098-013-0709-0.
16. D. Shao, D. Gao, Q. Wei, H. Zhu, L. Tao and M. Ge, *Appl. Surf. Sci.*, **257**, 1306 (2010); https://doi.org/10.1016/j.apsusc.2010.08.056.
17. M.A. Tavanaie, *Chem. Eng. Technol.*, **36**, 1823 (2013); https://doi.org/10.1002/ceat.201300146.
18. R. Wahab, A. Mishra, S.I. Yun, Y.S. Kim and H.S. Shin, *Appl. Microbiol. Biotechnol.*, **87**, 1917 (2010); https://doi.org/10.1007/s00253-010-2692-2.